# Fatigue performance of aircraft panels with novel skin buckling containment features

Quinn, D., Murphy, A., & Cervi, L. (2011). Fatigue performance of aircraft panels with novel skin buckling containment features. Proceedings of the Institution of Mechanical Engineers, Part G: Journal of Aerospace Engineering, 225(7), 791-806. DOI: 10.1177/0954410011399035

**Published in:**
Proceedings of the Institution of Mechanical Engineers, Part G: Journal of Aerospace Engineering

**Document Version:**
Peer reviewed version

**Queen's University Belfast - Research Portal:**
Link to publication record in Queen's University Belfast Research Portal

# Fatigue performance of aircraft panels with novel skin buckling containment features

D. Quinn[a], A. Murphy[a,*] and L. Cervi[b]

[a] *School of Mechanical and Aerospace Engineering, Queen's University Belfast, Ashby Building, Belfast. N. Ireland, U.K. BT9 5AH*

[b] *Unité Aéronautique et Laminés Technique, Centre de Recherche de Voreppe Centr'Alp, BP 27, 38341 Voreppe Cedex France*

## Abstract

To increase the structural efficiency of aircraft stiffened panels it is plausible to introduce skin buckling containment features to increase the local skin stability and thus static strength performance. Introducing buckling containment features may also significantly influence the fatigue crack growth performance of the stiffened panel. The focus of this article is the experimental demonstration of panel durability with skin bay buckling containment features. Through a series of fatigue crack growth tests on integrally machined aluminium alloy stiffened panels, the potential to simultaneously improve static strength performance and crack propagation behaviour is demonstrated. The introduction of prismatic buckling containment features which have yielded significant static strength performance gains have herein demonstrated potential fatigue life gains of up to +63%.

**Keywords:** Fatigue crack growth, integrally machined, stiffened panels, buckling containment features, experimental test.

*** Corresponding author:** Tel.: +44 (0) 28 9097 4095; fax: +44 (0) 28 9066 1729. E-mail address: a.murphy@qub.ac.uk (Adrian Murphy).

# 1 Introduction

## *1.1 Overview*

Stiffened panel buckling containment features and fatigue crack growth containment features have the potential to improve metallic panel durability and static strength. The latest generations of manufacturing technologies such as high speed machining, welding and panel extrusion, establish the potential to produce novel panel designs with integral containment features at low cost. As will be demonstrated within the following literature review sections, significant work has been undertaken to understand the physical behaviour and potential benefits of introducing skin fatigue crack growth and buckling containment features. However, little data is available on the interaction of fatigue crack growth containment features on stability performance, or buckling containment features on panel fatigue crack growth performance. Hence, this paper presents the findings of an experimental fatigue test programme which examines the fatigue crack growth behaviour of a skin crack under a broken stringer within a representative aircraft fuselage panel containing skin buckling containment features.

The experimental programme aims to demonstrate the potential to introduce buckling containment features without degrading panel durability, and to generate experimental data which can be used to validate modelling techniques to predict crack growth through both buckling and crack propagation containment features. The stiffened panel designs examined herein are derived from experimental and computational static strength and stability analysis undertaken in previous research [1, 2]. These panels have been designed primarily considering their static strength performance, which includes all forms of structural failure induced by static loading.

### *1.2 Paper synopsis*

The article is organised as follows: the following section introduces aircraft stiffened panel design and work to date to improve durability and stability through the introduction of skin bay local design features. The following section then introduces the stiffened panel designs to be experimentally examined herein, including the results of their static strength testing. Section 4 introduces the fatigue specimens, representing the aforementioned stiffened panel designs, plus key details on specimen manufacture, preparation for test and test procedure. Section 5 delivers the experimental results and Section 6 discusses these. Section 7 concludes the article with a summary of the key findings.

## 2 Background

### *2.1 Stiffened panel design*

Thin-walled stiffened panels have been employed in the manufacture of aircraft primary structures for more than 50 years. The structural performance, and hence design, of such panels is driven by a combination of static strength and durability requirements. With the objective to design panels of minimum weight, that satisfies the static strength and durability requirements, using manufacturing processes with tolerable production risk and capable of generating components at an acceptable cost. Stability performance is typically the key driver for structures which are heavily loaded in compression and or shear, with structural durability then checked with respect to fatigue, damage tolerance and fail-safe behaviour. For structures predominately loaded in tension, the durability requirements are the key design drivers, integrated with in-service inspection and maintenance targets, along with satisfying static strength.

Over this lengthy period of time significant improvement has been made in terms of metallic material properties, both with respect to static strength and durability. Combined, these developments have resulted in generations of light-weight assembled panel solutions. With improved material static strength enabling thinner panel elements and improved durability allowing higher working stresses and thus the thinner panel elements.

Considering manufacturing developments, significant progress in reducing the manual labour required within panel assembly has been achieved. With today's processes capable of cost effectively producing high tolerance very thin-walled panels. For future panel manufacturing, unitised structures have the potential to bring benefits with regards reduced part count, weight savings through the reduction of structural joints and simplification of in-service inspection. Such unitised structures can be realised for metallic panels via a combination of processes such as extruding, welding, high-speed machining plus advanced forming methods, rather than the traditional riveting processes [3-5]. Such processes bring the additional potential benefits of lower assembly times and thus lower manufacturing unit costs.

In embracing new manufacturing processes to produce integral panels, the potential to cost effectively include complex skin and stiffener cross-sections are introduced. Such complex skin and stiffener profiles have been proposed to contain crack propagation behaviour [6-7] and to improve local skin buckling behaviour [8-9]. The concept of local panel cross-section profiling can comprise anything from local increases in skin thickness to the introduction of small integral stiffeners between larger primary stiffeners, Figure 1. In reality, for aerospace applications, such features must address both strength and durability; in zones heavily loaded in compression and or shear they must improve stability and have at least a neutral influence

on durability. In zones predominately loaded in tension, local skin and stiffener profiling must improve durability and have at least a neutral effect on stability.

### *2.3 Improving stiffened panel durability*

While integral panel components are employed in current aircraft, the application of large scale integral structures has been inhibited as they do not contain redundant structural members that could act as retarders or crack stoppers. As noted before, material advances have seen improved damage growth (e.g. $K_{IC}$) and toughness properties (e.g. $G_{IC}$), resulting in the potential for more fatigue resistant and damage tolerance structures. The improvements are significant, particularly when referenced to benchmark aerospace material technology, such as 2024 and 7075 which are common in aircraft flying today, Table 1. However, alone these improvements do not meet the standards set by composite materials, where traditional airframe structures need to display an increase of 30% higher toughness to be considered competitive [7]. This deficit can not be closed through advanced aluminium alloys alone. Therefore significant research effort has been focused on novel stiffened panel design features to improved durability.

A promising practical solution to overcome the disadvantages of a fully unitised structure is the use of bonded crack containment features, Figure 1. Numerous bonded feature types and materials (aluminium, titanium, glass fibre metal laminate, carbon fibre polymer laminate) have been examined. Based on experimental and analytical results significant benefit in terms of reduced crack growth rates and improved fail safe behaviour have been demonstrated [9-16]. For example, experimental analysis of integral metallic panels with Glare reinforcement straps [9] indicate potential residual strength increases of 25 to 40%, and potential weight savings of up to 30%, when applied to damage tolerance critical areas.

The crack containment features retard crack growth by first providing local stiffening when a crack within the panel approaches and subsequently propagates beneath the bonded feature. The local stiffening of the bonded feature, by transferring load from the cracked panel, locally reduces crack loading and hence crack growth. Once the crack has passed beneath the bonded feature a complete load path remains intact behind the crack tip, so-called 'crack bridging', reducing the crack opening displacement and hence the crack growth.

Such a hybrid panel structure could result in reduced assembly complexity over a riveted built-up panel, but potentially with a higher manufacturing time, cost and in-service inspection complexity than a fully unitised structure. Moreover, in bonding and the use of dissimilar materials, the mechanics of failure are more complicated and varied. Potential modes of failure include adhesive interface disbond, bonded feature delamination and fatigue failure [16]. In addition, the presence of local thermal residual stresses, arising from bonding and curing, have been demonstrated to significantly influence fatigue performance.

Combining the concept of crack containment features and embracing the full potential of new manufacturing methods, which can cost effectively introduce complex skin and stiffener cross-sections, integral panels with built-in crack containment features have been conceived and demonstrated. Studies by Muzzolini [7], further developed by Ehrstrom [17], focused on improving fatigue crack growth behaviour by altering the skin cross-section between panel primary stiffeners. Experimental and numerical studies indicate that multiple regions of thickness variation, or crenulations, that are dimensionally wider than they are thicker, offer the greatest potential for improved life performance, Figure 1. It is proposed that the crack retardation effects operate on the principle of varying stress intensity across the panel skin bays, whereby stress intensity reduces as the crack progresses into a design feature and

increases as the crack leaves the feature. If designed correctly, over the panel skin the reduction in stress intensity and reduced crack growth rate outweighs the increase in stress intensity and increased crack growth rate [6, 9, 17]. Fatigue life gains of up to 100% or allowable stress gains of up to 15% over mass equivalent panels without integral damage containment features have been demonstrated [7, 9, 17].

The use of integral damage containment features clearly utilises the potential of new manufacturing methods in improving fatigue crack growth behaviour within unitised stiffened panels. However it is worth noting, a unitised stiffened panel with integral damage containment features does not contain discrete structural members which have the potential to act as discrete crack stoppers as would be found within a traditional built-up panel, assembled with mechanical fasteners.

### *2.4 Stiffened panel stability*

Up to this point the novel panel designs being explored are aimed at improving fatigue performance through crack retardation, however, there is also the potential to apply similar cross-section or profile features which would improve panel static strength and in particular panel stability behaviour.

Considering integral design features, the influence of simple geometric variation on plate stability performance has been examined extensively [18-22]. Of particular interest is studies by Petrisic [22] investigating the influence of strengthening pads distributed across a plate. The investigation indicates potential performance gains of up to 100% under axial compression and 150% under shear loading.

Experimental and numerical studies into the buckling and importantly into the post-buckling performance of stiffened panels with 'crenulated' skin bays under axial compression have been carried out by Murphy [23]. The influence behind this work stems from crack growth retardation concepts investigated by Ehrstrom [17]. Experimental analysis demonstrated skin buckling gains of up to 15% and higher panel collapse loads of up to 10% are achievable for mass equivalent designs. Significantly, the experimental findings also demonstrated that poorly designed damage containment features can lead to deteriorated static strength performance.

Studies into variable stiffener height panels, considering the introduction of smaller sub-stiffeners on a skin bay between larger primary stiffeners, has also demonstrated static strength benefits [24-26]. Numerical optimisation studies exhibited mass savings of up to 8.2% over traditional stiffened panel designs [25], while at the same time offering more robust designs [24]. However, investigations by Watson [25] also suggest that the presence of stiffeners of variable height can introduce additional and more complex panel instability modes.

## 3 Static specimen design and test

### *3.1 Specimen design*

The static strength design activity produced three specimen designs, two with buckling containment features and one reference design with no containment features.

### *3.1.1 Reference panel design*

The reference design was constrained to represent a fuselage panel loading intensity, initial buckling to collapse strength ratio, stiffener to skin stiffening ratio and the inclusion of pad-ups under primary stiffeners, Figure 1, to facilitate future potential manufacturing processes such as laser beam welding. As the primary focus is panel skin behaviour, complex stiffeners were avoided by designing blade section stiffeners. Given the design targets and constraints the cross-section of the longitudinal stiffeners and the skin bay cross-section were sized using standard industrial aerospace static strength analysis methods [27-29].

A static test specimen configuration representing the reference panel design was then developed, with three longitudinal stiffeners and representing a single lateral stiffener bay, Static Test Specimen A (STS-A), Figure 2.

### *3.1.2 Prismatic panel design*

The first design incorporating buckling containment features, and embodied in Static Test Specimen B (STS-B), uses simple blade cross-section buckling containment features arranged in a prismatic planform, Figure 2. Imitating the reference specimen (STS-A) the design consists of three primary stiffeners, identical in profile and pitch to the reference design, with each skin bay modified with the buckling containment features. Considering a number of manufacturing and minimum thickness and maximum height constraints the skin bay buckling containment features were sized using analysis methods which evaluated local and global buckling modes, with the aim of maximising static strength performance with neutral weight change. The selected configuration resulted in a reduction of the reference skin thickness to allow the introduction of five blade section buckling containment features within

each skin bay and a mass equivalent panel cross-section (with a small tolerance given the applied manufacturing constraints).

### *3.1.3 Non-prismatic panel design*

Under pure compression loading, introducing features that longitudinally stiffen potentially offers the greatest overall benefit. However, aircraft stiffened panels typically have to cope with a variety of loading conditions, normally including combinations of destabilising compression, both laterally and longitudinally, shear and normal loading. Hence, the introduction of off-axis features is of great interest for tailoring to the particular loading environment. Thus, for biaxially loaded, stability critical applications a number of non-prismatic planforms were considered, inspired by the curvilinear patterns previously developed for metallic panels [30] and tow-steered composite panels [31-32], whereby locally increasing plate out-of-plane bending stiffness at 45 degree angles to the primary stiffeners can significantly improve plate stability performance. The outcome being a buckling containment feature topology aimed at application areas which are subjected to combinations of destabilising loading.

However, preliminary manufacturing simulations indicated significant additional machining time due to the high number of acute angles at the containment feature intersections. Thus a simplified configuration was developed based on an orthogonal pattern concept. The non-prismatic panel design, embodied in Static Test Specimen E (STS-E), used again simple blade cross-section skin buckling containment features, but with a non-prismatic stiffening planform, Figure 2. Given the simplified buckling containment feature topology the local skin geometry was sized for static strength, considering local skin bay and global panel buckling behaviour. The manufacturing constraints applied to the design of the reference and

prismatic panels (STS-A and STS-B) were again applied with the target of producing a mass equivalent panel design (again with a small tolerance considering practical machining increments). The detailed sizing resulted in a mass equivalent panel design but with a reduced skin thickness when compared with the reference design.

### *3.2 Static test results*

Before testing, each specimen had a reinforced epoxy resin base cast onto each end. Once cast each specimen was strain gauged and painted in preparation for test. Gauges were located to assist in the determination of initial skin buckling and post-buckling collapse behaviour. Specimen end-shortening was measured using two calibrated displacement transducers. These were located on either side of the specimen in the plane of the cross section neutral axis. Additionally, a three-dimensional Digital Image Correlation (DIC) system was used to capture skin deformation behaviour during the tests.

Table 2 presents the experimentally measured specimen masses, initial skin buckling and ultimate specimen collapse loads. The load versus end-shortening curves, illustrating specimen pre- and post-buckling stiffness are presented in Figure 3. The full test results are presented in detail in references [1] and [2] and in summary form here.

First, considering the panel design with prismatic buckling containment features versus the reference panel design with flat uniform thickness skin bays (specimen STS-B versus STS-A). The experimental results demonstrate the potential to improve skin element stability with mass equivalent design, Table 2. For the particular geometry and material tested, an initial skin buckling performance gain of +87.2% and resultant panel post-buckling collapse gain of +17.7% was measured [1]. Examining the physical behaviour of the two test specimens, the

presence of the buckling containment features has caused variation in the initial skin buckling form between the two specimens. The addition of the skin prismatic buckling containment features locally changed the out of plane bending stiffness, resulting in an increase in the skin buckling wavelength from that of the uniform thickness skin bay. This increase in skin buckle wavelength has been accompanied by an increase in the stress level to cause instability, and thus load required to cause initial buckling. In this particular example the prismatic skin buckling containment features of Specimen STS-B have forced the central line of the skin bay to behave more like a column, forming a single longitudinal half-wave buckle, Figure 3, this is in contrast to that observed in the uniform skin of Specimen STS-A, which initially buckled with three longitudinal half-waves.

Considering the panel design with non-prismatic buckling containment features versus the reference panel design (specimen STS-E versus STS-A). Again the experimental results demonstrate the potential to improve panel stability with measured initial skin buckling performance gains of +185.1% and resultant panel post-buckling collapse gains of +17.5% [2]. With regards to the physical behaviour of the test specimens, again the presence of the buckling containment features has caused variation to the initial skin buckling form. The addition of the non-prismatic buckling containment features has locally changed the skin out-of-plane bending stiffness, forcing the initial buckle half-waves to develop between the buckling containment features, which act as buckling inflexion lines. The result is a reduction in buckling wavelength, and thus an increase in the number of buckle half-waves on each skin bay, from three in Specimen STS-A to thirteen in Specimen STS-E, Figure 3.

Considering panel post-buckling behaviour for both the prismatic and non- prismatic buckling containment feature specimens, improved initial skin bay buckling increases both

the skin working stresses and the effective contribution of the skin to the panel post-buckled load carrying ability, thus increasing panel global collapse loads.

## 4 Fatigue specimen design, manufacture and test

The focus of this article is the experimental demonstration of panel durability with skin bay buckling containment features. The experimental programme examines the resistance to fatigue crack growth of the three previously developed panel designs, which were tested under static loading conditions as outlined in the proceeding section.

### *4.1 Reference specimen*

Fatigue Crack Growth specimen A (FCG-A) represents the reference panel design. The overall specimen geometry was sized to accommodate a skin crack under a broken central stiffener, with the broken stiffener bounded by intact stiffeners on either side. The global specimen dimensions were further confined by the width of the test machine grip, and available length of material (from the same batch as the static test specimens). Figure 4 presents the undamaged specimen geometry; with a test section measuring 295 mm in length. The specimen also replicates the material state and manufacturing method of the reference static test specimen (STS-A).

### *4.2 Prismatic panel design*

Fatigue Crack Growth specimen B (FCG-B) replicates the material, cross-sectional geometry and manufacturing method of the panel design with prismatic buckling containment features (as represented in the static test specimen STS-B). Again the fatigue specimen overall geometry was sized with respect to the test machine and available batch material, and with

the intent to accommodate an initial skin crack under a broken central stiffener bounded by intact stiffeners, Figure 4.

### *4.3 Non-prismatic panel design*

Fatigue Crack Growth specimen E (FCG-E) replicates the panel design with non-prismatic buckling containment features (as represented in the static test specimen STS-E). Again the specimen overall geometry was sized to accommodate a central stiffener and skin crack, the limits of the test machine and available batch material, Figure 4.

### *4.4 Manufacture*

The three fatigue specimens were manufactured through a CNC subtractive machining process on a Bridgeport 2.5D Vertical Milling Machine (VMC 1000/22) from 50mm thick Aluminium Alloy 2024-T351 plate. With regards to manufacturing precision, the completed specimens were measured for dimensional accuracy, using both CMM and digital micrometers, with all thickness and length dimensions found to lie within 0.5% of the specified design geometry.

### *4.5 Specimen preparation*

Prior to testing each specimen was pre-damaged using a wire EDM cutting process in accordance with ASTM procedures [33]. As demonstrated in Figure 5, an initial cut was centred at the midpoint of the central primary stiffener of each specimen, perpendicular to the loading axis, and measuring 24mm in length and 2mm in width. The initial crack length, $2a_0$, was selected based on a specimen half crack length to half specimen width ratio ($a_0/W$) of 0.1, typical of aerospace panel fatigue crack growth testing [12, 17]. The initial specimen cut was through the central primary stiffener, adjacent pad-up and skin containment features.

This is representative of aerospace testing procedures where crack propagation from a damaged stiffener across two adjacent skin bays is a critical design case [34]. The non-prismatic specimen, FCG-E was given a second pre-damage site. Located within the skin bay, adjacent to an outer primary stiffener and centralised between a set of off-axis buckling containment features, Figure 5. The two pre-damage sites were designed to observe crack behaviour at two distinct points of interest – a crack propagating towards an off-axis containment feature, and a crack propagating towards a containment feature intersection point.

### *4.6 Testing procedure*

Testing was carried out in a 2500 kN capacity universal hydraulic test machine at Alcan CRV, Voreppe, France. The specimens were secured between two clamping jaws, one jaw fixed and the other jaw displacing cyclically. The test setup was designed to facilitate the cyclic axial loading of the specimen while monitoring lateral crack growth. The specimens were subjected to typical metallic aircraft loading with a maximum stress level of 100 MPa at a stress amplitude ratio R of 0.1 [12, 35-36]. Cycling frequency (4Hz) and amplitude was digitally controlled with a reactive load cell providing load data. Each specimen underwent fluctuating tensile loading of constant amplitude until the crack propagated through a second primary stiffener.

For specimen FCG-A and FCG-B crack growth propagation was measured approximately every 500 cycles using an automated optical measurement system. For specimen FCG-E, in which crack behaviour at four distinct points was to be measured, a system with a reduced accuracy (+/-0.5mm) was used for measurement. This resulted in crack growth data for FCG-E at approximately an order of magnitude higher than for specimen FCG-A and FCG-B.

## 5. Experimental Results

### *5.1 FCG-A*

The experimentally measured crack length "a", as referenced from the initial damage, is presented in Figure 6 for both crack fronts. Crack directionality is referenced with the specimen test section viewed from the stiffener side. The measured crack growth rate is presented in Figure 7, calculated for the total crack length, "2a" and presented against the average half-crack length, "a", for ease of reference to the skin bay geometry. The calculation of crack growth rate exhibits a degree of "noise" that is related to the tolerance of the automated crack measurement system, particularly at lower values of crack length where the ratio of measurement accuracy (+/- 0.05mm) to crack length is high.

The crack demonstrates relatively symmetric growth about the central primary stiffener, with the exception of a marginal variation between approximately 35mm and 75mm. There appears to be a relatively linear acceleration of crack propagation across the skin bay, as demonstrated by the crack growth rate relationship, Figure 7. Between a crack length of 12mm and 140mm the approximate rate of increase of crack growth rate per unit increase in crack length is $1.9 \times 10^{-4}$. As the crack fronts approach the outer primary stiffener there is a considerable reduction in local crack growth rate. This replicates the crack growth retardation concepts were the presents of the pad-up and in this case a stiffener reduces the stress intensity as the crack progresses into the pad-up, reducing the local crack growth rate.

At 30,200 cycles the crack penetrates the right hand side stiffener pad-up and at 30,400 cycles the crack penetrates the right hand side stiffener pad-up. Specimen failure occurs at 31,700 cycles with complete rupture of the right hand side edge stiffener (viewed from the stiffener side). Failure corresponds to a sharp acceleration of crack growth as it propagates

past the centreline of the stiffener, Figure 7. At the point of failure, the corresponding crack on the left hand side stiffener has propagated approximately 75% of the stiffener web height. Figure 8 captures the specimen at the point of failure. With regards to crack growth direction, the crack fronts remain perpendicular to the primary stiffeners with a maximum vertical deviation of +/- 4mm (0.68% of the specimen height) relative to the plane of the initial crack.

### *5.2 FCG-B*

During the initial testing of FCG-B an unplanned overload, with a 100% increase in the maximum stress level, oscillating between 200 MPa and 20 MPa, was applied for the first 500 cycles. The maximum overload stress was elastic (64.5% of 0.2% yield stress) and as such did not induce any widespread plastic deformation on the specimen. The effect of the increase in stress is to increase in size the plastic zone in front of the crack tips, producing a region where the crack growth rate is significantly lower than under the normal test conditions. Using conservative calculations of the radius of the plastic zone [37], the specimen underwent cyclic loading at the correct stress range until the crack propagated beyond the induced plastic zone and a steady crack growth rate was observed. At this point the test was continued, with the cycle count restarted, essentially carrying out a standard test with a larger initial crack length, "2a", increased from 24mm to 38mm. The measured crack lengths for this specimen, as presented in Figure 9, are referenced from the increased initial crack. As before crack directionality is referenced with the specimen test section viewed from the stiffener side. Figure 7 also presents the measured crack propagation rate, calculated for the total crack length, "2a" and presented against the average half-crack length, "a", again for ease of reference to the skin bay geometry. As before the calculation of crack growth rate exhibits a degree of "noise" that is related to the tolerance of the automated crack measurement system.

The crack propagation behaviour of the left and right hand side crack fronts of the specimen are relatively symmetric about the central primary stiffener. There is evidence of a change in the crack growth as it propagates through the buckling containment features. Inspecting the crack growth rate behaviour, Figure 7, the global trend is an overall acceleration across the skin bays, with a global slope not dissimilar to the reference specimen results (FCG-A). However, there are distinct local oscillatory trends as the crack decelerates on approach to each buckling containment feature and then accelerates on exiting each feature. It is worth noting that through crack rupture of each buckling containment feature occurs approximately 1,000 cycles after the crack, viewed from the skin side, passes underneath the buckling containment feature. Examining the crack growth rate data versus crack length data, the retardation effect of the buckling containment features appears to begin around the centre line of the sub-bays, with the acceleration post containment feature stabilising again around the centre line of the sub-bays.

While each buckling containment feature appears to temporarily slow crack propagation, the degree of crack retardation reduces as the crack progresses across the skin bay. As the crack approaches the outer primary stiffeners the crack growth rate slows, and within 20mm of the outer primary stiffener centreline, the crack growth rate behaviour is consistent with the reference specimen. At 41,800 cycles the crack penetrates the left hand side stiffener pad-up and at 42,000 cycles the crack penetrates the right hand side stiffener pad-up. Specimen failure occurs at 43,550 cycles with rupture of the right hand side primary stiffener, viewed from the stiffener side. An image of the specimen captured at the point of failure is presented in Figure 8. At the point of failure, the left hand side crack has propagated approximately 25% up the primary stiffener web. With regards to crack growth direction, the crack fronts

remain perpendicular to the primary stiffeners with a maximum vertical deviation of +/- 2mm (0.34% of the specimen height) relative to the plane of the initial crack.

### *5.3 FCG-E*

The experimentally measured crack length "a", as referenced from the initial damage, is presented in Figure 10 for both individual crack fronts at both the primary and secondary pre-damaged sites (sites A and B respectively in Figure 5). Due to the reduced resolution and the precision of the crack length measurement for this specimen, an accurate representation of the crack propagation rate can not be presented.

Considering the primary central crack, the crack growth behaviour displays two distinct trends. There appears to be a general reduction or slowing of the crack growth as it progresses towards the intersecting buckling containment features. Upon entering the second sub-bay there is a distinct acceleration of crack growth. The crack grows straight through the intersection into the adjacent sub-bay, with complete rupture of the buckling containment feature occurring at 14,500 cycles. At a total crack length, "2a", of 163mm (16,500 cycles) an attempt was made to arrest the primary central crack. The attempt to arrest the primary central crack involved drilling a 4 mm diameter hole at each crack front, the hole edges were subsequently polished before testing was resumed. This approach is appropriate to arrest cracks during test when crack growth remote from the area of interest is found and where patching would significantly alter the loading within the area of interest. The purpose of arresting the central crack was to permit further growth of the secondary edge crack (site B, Figure 5), which had exhibited slower crack growth, without the central crack propagating to the point of specimen failure.

Considering the secondary edge crack, the growth rate was relatively stable for the duration of the test. The magnitude of the edge crack length was 17.2% of the corresponding central crack length when the arrest of the central crack was attempted. As the crack progressed towards the buckling containment features there appears to be a marginal acceleration of the crack growth rate. With regards to the crack growth direction, the crack does not remain perpendicular to the loading direction, Figure 11. The crack front growing towards the centre of the specimen turns towards the upward off-axis buckling containment feature, while the crack growing towards the edge of the specimen turns downward becoming less perpendicular to the primary stiffeners.

The attempt to arrest the primary central crack proved unsuccessful and the central crack continued to propagate. Consequently the cyclic loading was terminated and presented crack length data for FCG-E does not extend beyond the point of attempted crack arrest. However, to qualitatively observe the residual strength failure behaviour of a panel with non-prismatic buckling containment features, the specimen was subjected to an ultimate uniform tension test. As demonstrated in Figure 8, the specimen exhibits signs of crack turning on tension failure. On the left hand side (viewed from the stiffener side) there is interaction of the secondary edge and primary central crack fronts, with the central crack turning upwards towards the edge crack. On the right hand side the central crack front turns and propagates along a buckling containment feature adjacent to the outer primary stiffener.

## 6.0 Discussion

### *6.1 Data correction for comparison*

For the purpose of comparing the relative performance of the specimens it is necessary to correct for the initial over-load experienced by FCG-B. Two correction procedures can be considered to permit the crack growth behaviour to be referenced from an equivalent initial crack length. The first correction procedure simply represents the crack growth behaviour for all specimens from the "new" initial crack length of FCG-B (38mm). The second correction procedure linearly interpolates the crack growth behaviour of FCG-B backwards to the originally designed initial crack length (24mm). Table 3 presents the number of cycles for the cracks to propagate across the specimen as corrected using both methods. For a uniform thickness skin bay, where the crack growth rate is relatively linear, the interpolation of crack behaviour backwards to an initial crack length is obvious. Considering the variable propagation rate of specimens containing containment features, such an interpolation is less robust. Thus Figure 12 presents the total crack length, "2a", for all specimens as corrected for an equivalent initial crack length of 38mm.

### *6.2 Panel design with prismatic buckling containment features*

Considering the performance of FCG-B relative to FCG-A, Figure 12, the specimen with the prismatic buckling containment features yielded an increase of +63.1% in cycles required to cause failure (when cycles are referenced from the "new" crack length of 38mm). The crack growth rates between containment features oscillate both above and below that of the uniform thickness design at the same location. However, the local reductions in fatigue crack growth approaching the containment features outweigh the increase in the crack growth rate as it passes through the containment features, Figure 7. The net result is an overall reduction in crack propagation rate across the skin bays, yielding the improved fatigue life of FCG-B.

The observed behaviour indicates a combination of effects by the buckling containment features. First the features periodically reinforce the skin thus varying the stress intensity across the skin bay and this causes the crack propagation rate to vary. The design is such that across the skin bay the combined reductions in crack growth rate, associated with approaching a feature, outweighs the combined increase in crack growth rate associated with exiting a feature. Additionally, once the crack has passed beneath the individual buckling containment features the intact section of the feature bridges the crack reducing the opening displacement and further slows the growth. This occurs until the feature has been completely cracked through.

### *6.3 Panel design with non-prismatic buckling containment features*

Due to the premature conclusion of the fatigue testing of FCG-E, a direct comparison of specimen failure performance was not obtained. However, with the experimental data available there are a number of observations that can be made.

The initial growth rate of the central crack (<5,000 cycles) appears higher than that of the reference and prismatic buckling containment feature designs, Figure 10. Considering the local skin designs, the skin and containment feature thicknesses for both buckling containment designs are identical. Moreover the distance from the initial central crack to the first containment feature is similar, 31.9mm for FCG-B and 33.7mm for FCG-E. Therefore, the apparent higher initial crack propagation rate of FCG-E may arise not from local design differences but from global differences. While the average cross sectional area of all designs is equivalent, the cross-sectional area varies for the non-prismatic design, Figure 4. In the plane of the specimen central crack, Figure 5, the cross sectional area is lower than the design average. Thus higher stress intensity in the plane of the crack may have induced a higher

propagation rate. In addition, the varying cross sectional geometry also causes the local neutral axis to shift through the design, with potential bending effects also inducing higher local stresses.

In the proximity of the containment feature intersection the crack growth behaviour displays similarities to that of the prismatic containment feature design, Figure 10. Approaching the feature there appears to be a reduction in the crack growth rate, and as the crack propagates through the feature the crack growth accelerates. The crack appears to approach the containment feature at a rate similar to that of FCG-B, however, it appears to accelerate away at a much greater rate. Again, the higher propagation rate may be due to the reduced cross section, and in addition perhaps the size of the adjacent skin "sub-bay", with the crack passing through a containment feature on FCG-B having a shorter pitch to propagate to the next containment feature than on FCG-E.

The secondary edge crack on FCG-E exhibits slower crack growth behaviour than the primary central crack, Figure 10. Potentially due to the intact surrounding stiffeners, redistributing the load in the vicinity of the crack, preventing it from propagating at a speed similar to the central crack. However, the edge crack demonstrates signs of crack turning towards the off-axis buckling containment feature, Figure 11. Whether the turning effect is due to the presence of the central crack or the off-axis containment feature is still unclear, and requires further investigation.

## 7.0 Conclusions

The potential of introducing prismatic and non-prismatic buckling containment features to improve the static strength and stability of aerospace panels has previously been demonstrated. The work presented herein demonstrates through experimental analysis that buckling containment feature panel designs, driven by static strength and stability, can also yield improved crack propagation behaviour, essentially offering the potential to tailor panel skin bay geometry for both static strength and fatigue life. The experimental work focused on the design, manufacture and testing of three integrally machined aluminium alloy specimens under constant amplitude cyclic loading, monitoring lateral crack propagation across a test section comprising three primary stiffeners and two closed skin bays.

The introduction of prismatic blade profile skin buckling containment features demonstrated fatigue life performance gains of up to +63.1% over a conventional stiffened panel design. The presence of the prismatic buckling containment features produced crack growth acceleration and deceleration as a crack propagated across a skin bay, with the net outcome an overall reduced crack propagation rate. Experimental observations also indicate that the introduction of a non-prismatic buckling containment feature topology can have a detrimental influence on fatigue crack growth performance. The reduced local cross section and increased containment feature pitch within the non-prismatic design may have contributed to the reduced fatigue performance. Further work is underway to use the experimental work herein to validate crack growth prediction models, which will then be used to further the understanding of crack behaviour within panels with buckling containment features and assist in their future design.

Both static strength performance under compression loading and crack propagation performance under cyclic tension loading of stiffened panels may be influenced by local skin design. In the case of compression loading the out-of-plane bending resistance of the skin influences initial buckling behaviour. For cyclic tension loading, varying the stress intensity in the path of the crack influences propagation behaviour. Although there is no physical dependency between the stability and crack growth behaviour the out-of-plane bending resistance of the skin as well as the local stress intensity across the skin are both heavily influenced by any skin containment feature design. It thus becomes very important to design any buckling containment features with due consideration of fatigue crack growth performance, and conversely, design any fatigue crack growth containment features with due consideration of buckling performance.



**Acknowledgements**

The authors gratefully acknowledge the technical and financial support of Alcan CRV, Voreppe, France.

**References**


[1] Quinn D, Murphy A, McEwan W and Lemaitre F. Stiffened Panel Stability Behaviour and Performance Gains with Plate Prismatic Sub-Stiffening, Thin-Walled Struct 2009;47(12):1457–68.

[2] Quinn D, Murphy A, McEwan W and Lemaitre F. Non-Prismatic Sub-Stiffening for Stiffened Panel Plates – Stability Behaviour and Performance Gains, Thin-Walled Struct 2010; 48(6): 401-413.

[3] Munroe J, Wilkins K, Gruber M. Integral Airframe Structures (IAS) – Validated feasibility study of integrally stiffened metallic fuselage panels for reducing manufacturing costs. NASA Contractor Report, May 2000, NASA/CR-2000-209337.

[4] Pettit RG, Wang JJ, Toh C. Validated feasibility study of integrally stiffened metallic fuselage panels for reducing manufacturing costs. NASA Contractor Report, May 2000, NASA/CR-2000-209342.

[5] Metschan S. Validated feasibility study of integrally stiffened metallic fuselage panels for reducing manufacturing costs, cost assessment of manufacturing/design concepts. NASA Contractor Report, February 2000, NASA/CR-2000-209343.

[6] Lequeu P, Danielou A. Innovative High Perfromance Wing Concepts. Presented at the 17th Advanced Aerospace Materials & Processes Conference and Exposition (AeroMat 2006), 15-18 May 2006, Seattle, USA.

[7] Muzzolini R, Ehrstrom J.C. Damage tolerance of integral structures with crack retardation features. Presented at the 15th Advanced Aerospace Materials & Processes Conference and Exposition (AeroMat 2004), 7-10 June 2004, Seattle, USA.

[8] Ozakca M, Murphy A, Van Der Veen S. Buckling and Post-Buckling of Sub-Stiffened or Locally Tailored Aluminium Panels. 25th International Congress of the Aeronautical Sciences, 3-8 September 2006, Hamberg, Germany

[9] Bucci R.J. Advanced Metallic and Hybrid Structural Concepts: Tailorable solutions to meet the demanding performance/affordability requirements of tomorrow's aircraft.

Presented at the Aircraft Structural Integrity Program Conference (ASIP 2006), 28-30 November 2006, San Antonio, Texas.

[10] Farley G.L., Newman J.A., James M.A., Selective Reinforcement To Improve Fracture Toughness And Fatigue Crack Growth Resistance In Metallic Structures. 45th AIAA/ASME/ASCE/AHS/ASC Structures, Structural Dynamics & Materials Conference, 19 - 22 April 2004, Palm Springs, California, AIAA 2004-1924.

[11] Schijve J. Crack stoppers and ARALL laminates. Engng Fract Mech 1990;37(2):405–21.

[12] Zhang X, Li Y. Damage tolerance and fail-safety of welded aircraft wing panels. AIAA J 2005;43:1613–23.

[13] Gunnink J.W. Hybrid Structures: The new standard for Advanced Primary Aircraft Structures. Presented at the 18th Advanced Aerospace Materials & Processes Conference and Exposition (AeroMat 2007), 25-28 June 2007, Baltimore, USA.

[14] Heinimann M, Bucci R.J, Roebroeks G.H. Advanced Hybrid Structural Concepts for Care-Free Structures: Experimental Validation and Path Forward. Presented at the Aircraft Structural Integrity Program Conference (ASIP 2007), 4-6 December 2007, Palm Springs, California.

[15] Roebroeks G.H, Hooijmeijer P.A, Kroon E.J, Heinimann M.B. The Development of CentrAL. The First International Conference on Damage Tolerance of Aircraft Structures, 25-28 September 2007, Delft, Netherlands.

[16] Zhang X, Boscolo M. Fail-Safe Design of Integral Metallic Aircraft Structures Reinforced by Bonded Crack Retarders. Engng Fract Mech 2009;76:114-133

[17] Ehrström J.C, Van der Veen S, Arsène S, Muzzolini R. Improving damage tolerance of integrally machined panels. The 23rd Symposium of International Committee on Aeronautical Fatigue (ICAF 2005), 6-10 June 2005, Hamburg, Germany.

[18] Farley G. Selective Reinforcement to Enhance the Structural Performance of Metallic Compression Panels. 45th AIAA/ ASME/ ASCE/AHS/ASC Structures, Structural Dynamics & Materials Conference, 19 - 22 April 2004, Palm Springs, California.

[19] Biggers S.B, Srinivasan S. Compression Buckling Response of Tailored Rectangular Composite Plates. AIAA Journal Vol. 31(3) March 1993.

[20] Eisenberger M, Alexandrov A. Buckling Loads of Variable Thickness Thin Isotropic Plates. Thin-Walled Struct 2003;41(9):871–89.

[21] Baranski A.T, Biggers S.B. Postbuckling analysis of tailored composite plates with progressive damage. Comp Struct 1999:46:245-55.

[22] Petrisic J, Kosel F, Bremec B, Buckling of plates with strengthenings. Thin-Walled Struct 2006;44:334-343.

[23] Murphy A, Quinn D, Mawhinney P, Ozakça M, van der Veen S. Tailoring static strength performance of metallic stiffened panels by selective local sub-stiffening. 47th AIAA/ASME/ASCE/AHS/ASC Structures, Structural Dynamics, and Materials Conference, 1-4 May 2006, Newport, Rhode Island, AIAA-2006-1944

[24] Bushnell D and Rankin C. Optimum design of stiffened panels with sub-stiffeners. 46th AIAA/ASME/ASCE/AHS/ASC Structures, Structural Dynamics & Materials Conference, 18-21 April 2005, Austin, Texas, AIAA 2005-1932.

[25] Watson A, Featherston CA and Kennedy D. Optimization of postbuckled stiffened panels with multiple stiffener sizes. 48th AIAA/ASME/ASCE/AHS/ASC Structures, Structural Dynamics, and Materials Conference, 23-26 April 2007, Honolulu, Hawaii, AIAA 2007-2207.

[26] Maloney J, Chauncey Wu K, Robinson J. Analytical Comparison of Three Stiffened Panel Concepts. NASA Technical Memorandum 110165, Dec 1995.

[27] Bruhn EF. Analysis and Design of Flight Vehicle Structures. 1st Edition, Tri-State Offset Company, 1973.

[28] NASA. NASA astronautics structures manual, vol. 3. NASA, Washington, US, 1961.

[29] ESDU structures sub-series, Engineering Sciences Data Units, ESDU International Ltd.

[30] Kapania R, Li J, Kapoor H. Optimal Design of Unitized Panels with Curvilinear Stiffeners, 5Th Aviation Technology, Integration and Operations Conference (ATIO), Arlington, Virginia, September 2005.

[31] Waldhart C, Gurdal Z, Ribbens C. Analysis of tow placed, parallel fiber, variable stiffness laminates. 37th AIAA/ASME/ASCE/AHS/ASC Structures, Structural Dynamics, and Materials Conference, 15-17 April 1996, Salt Lake City, USA, AIAA-96-1569.

[32] Tatting B.F, Gurdal Z. Design and Manufacture of Elastically Tailored Tow Placed Plates. NASA Contractor Report, August 2002, NASA/CR-2002-211919.

[33] ASTM E647-00. Standard test method for measurement of fatigue crack growth rates. In: Annual book of ASTM standards 2002;03.01.

[34] Nesterenko G. Designing the airplane structure for high durability. AIAA/ICAS International Air and Space Symposium and Exposition, 14-17 July 2003, Dayton, Ohio, USA, AIAA-2003-2785.

[35] Llopart Ll, Kurz B, Wellhausen C, Anglada M, Drechsler K, Wolf K. Investigation of fatigue crack growth and crack turning on integral stiffened structures under mode I loading. Engng Fract Mech 2006;73:2139–52.

[36] Uz M-V, Kocak M, Lemaitre F, Ehrstrom J-C, Kempa S, Bron F. Improvement of damage tolerance of laser beam welded stiffened panels for airframes via local engineering. Int J Fatigue 2009;31:916-26.

[37] Anderson T.L. Fracture Mechanics: Fundamentals and Applications. 3rd Edition, Taylor & Francis, 2005, ISBN 9780849316562

| **Materials** | **2024A-T351** | **7449-T7951** | **6156-T6** |
|---|---|---|---|
| Application (large commercial transports) | Lower wing skin | Upper wing skin | Fuselage skin |
| Strength | Equivalent to 2024-T351 | +20% relative to 7075-T651; +10% relative to 7150-T651 | +10% relative to 2024-T3 |
| Damage tolerance | +30% relative to 2024-T351 | +10% relative to 7150-T651 | +25% relative to 2024-T3 |

**Table 1** Relative properties of the latest available aerospace aluminium alloys relative to the benchmark materials (2024, 7075 and 7150)

| | Manufactured mass (kg) | Initial plate buckling load (kN) | Ultimate panel collapse load (kN) |
|---|---|---|---|
| STS-A | 2.008 | 74.9 | 216.6 |
| STS-B | 1.981 | 140.2 | 255.0 |
| STS-E | 1.980 | 213.5 | 254.6 |

**Table 2** Static specimen mass and measured initial plate buckling and ultimate panel collapse loads

| | Number of Cycles to Failure | |
|---|---|---|
| | Referenced initial crack length 24mm | Referenced initial crack length 38mm |
| FCG-A | 31700 | 26697 |
| FCG-B | 57573 | 43550 |

**Table 3** Specimen cycles to failure after correction.

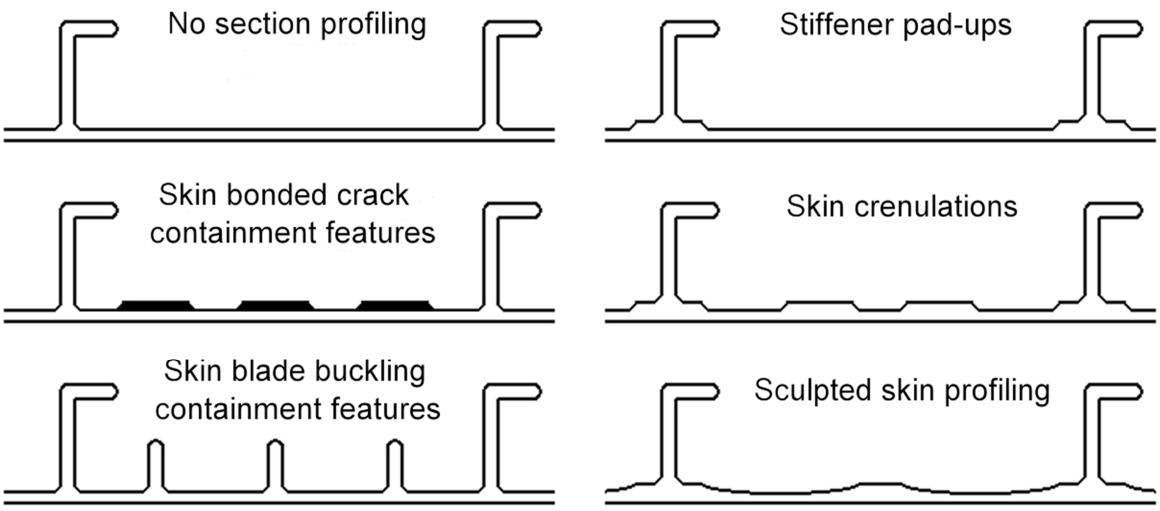


**Figure 1** Proposed fatigue crack growth and buckling containment feature.

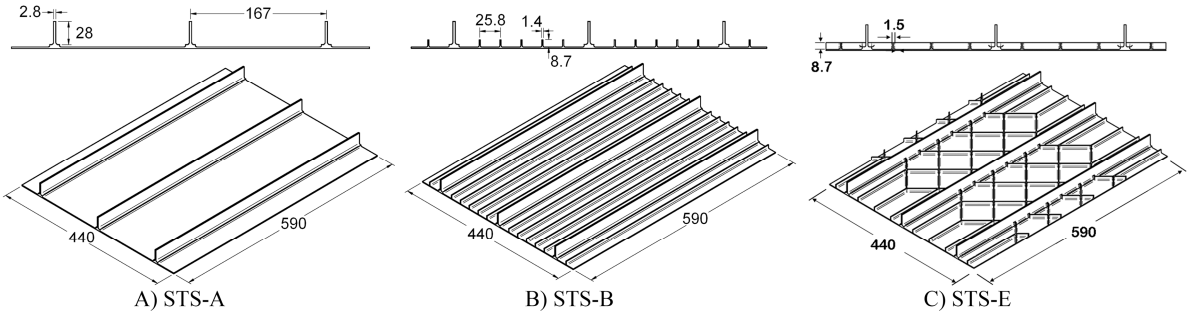


A) STS-A B) STS-B C) STS-E

**Figure 2** Static test specimen geometry.

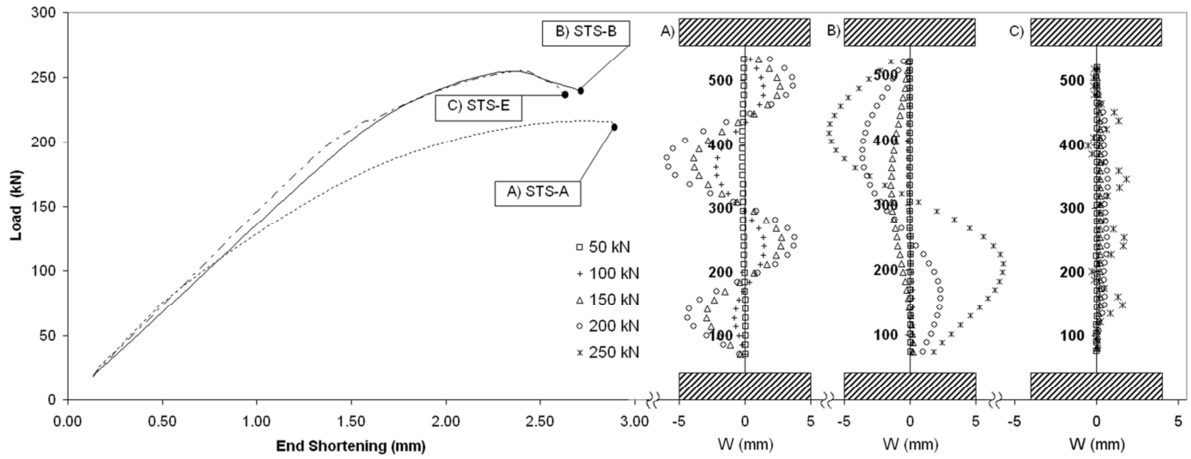


**Figure 3** Static test load deflection curves and skin out-of-plane deflection data.

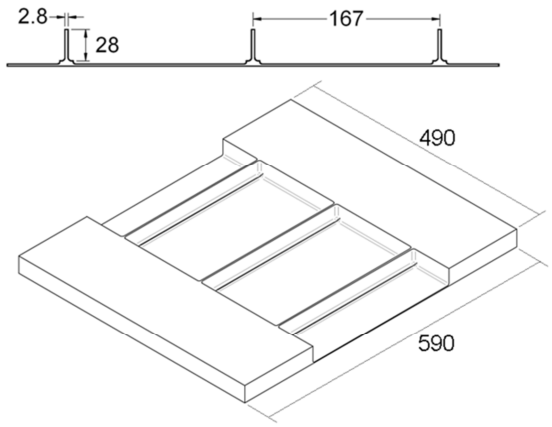


FCG-A

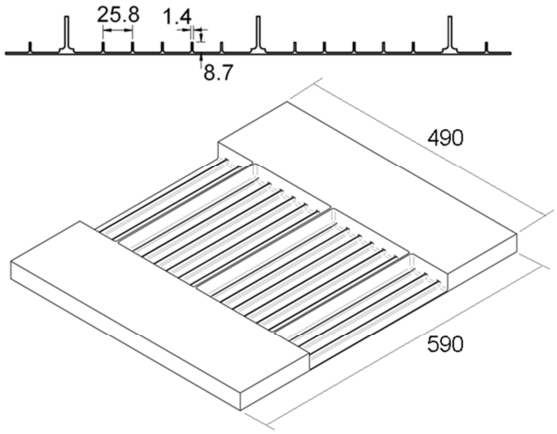


FCG-B

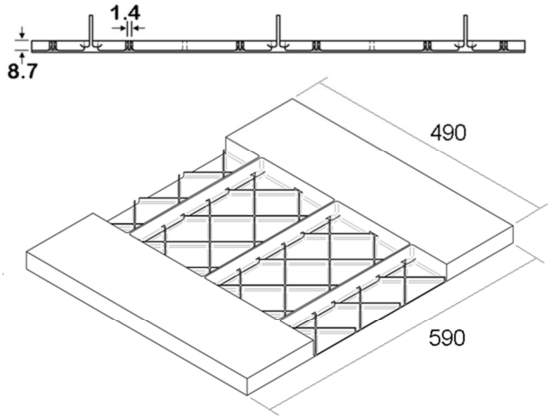


FCG-E

**Figure 4** Crack growth test specimen geometry.

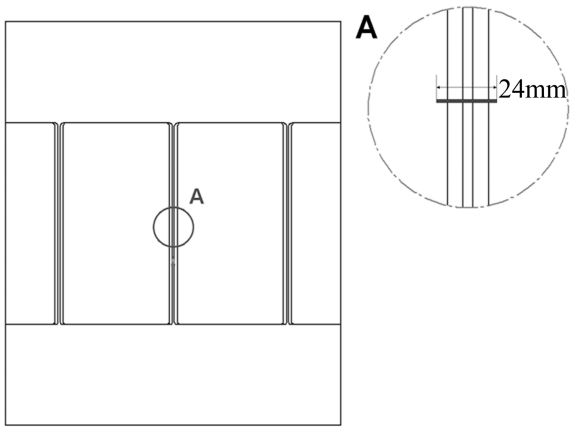


FCG-A

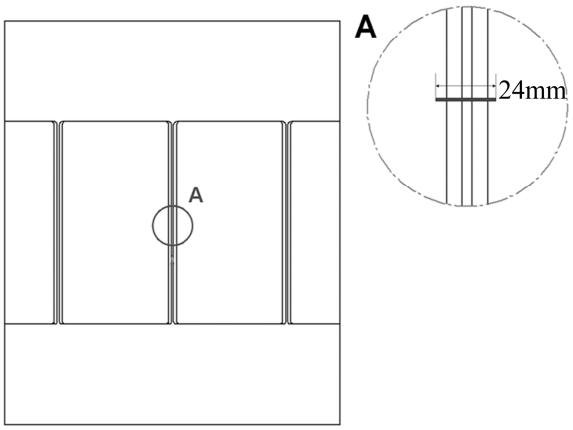


FCG-B

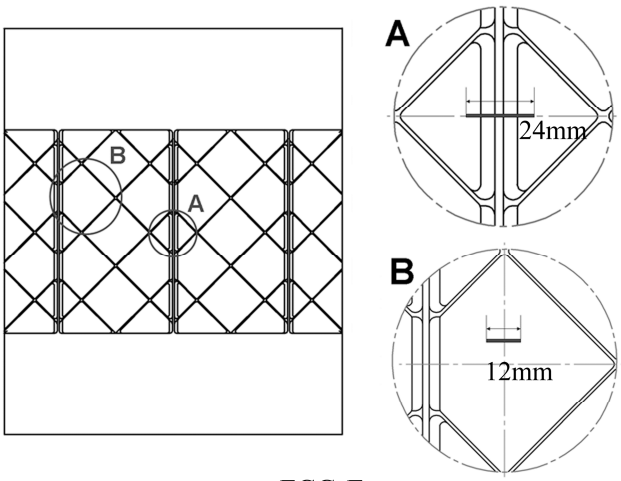


FCG-E

**Figure 5** Locations of the pre-damaged initial cracks.

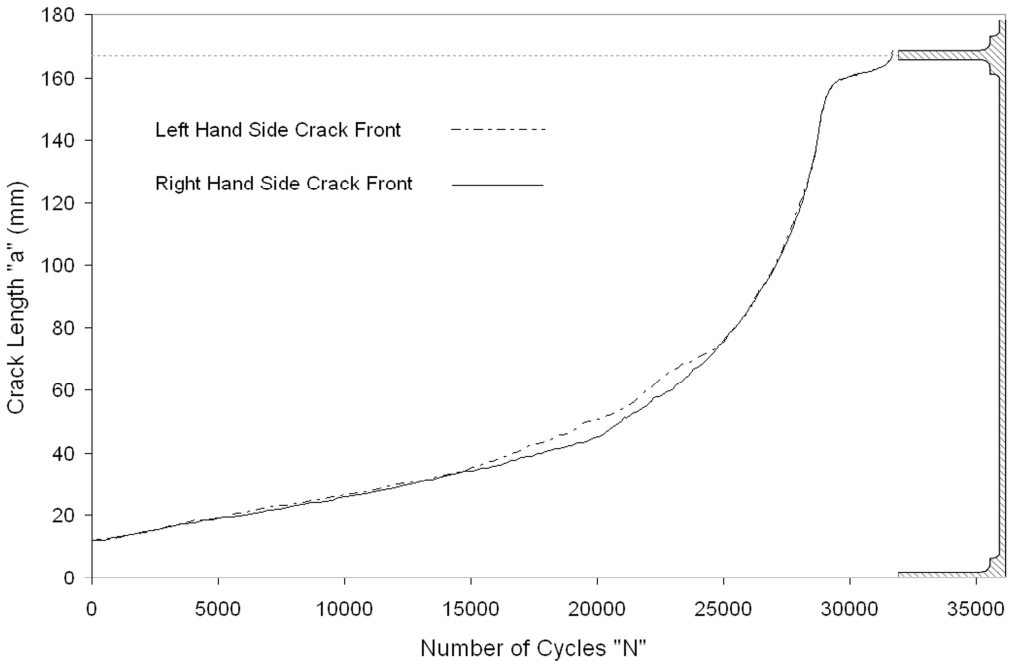


**Figure 6** Measured crack lengths of the two crack fronts on FCG-A across the skin bays. Direction referenced from the stiffener side.

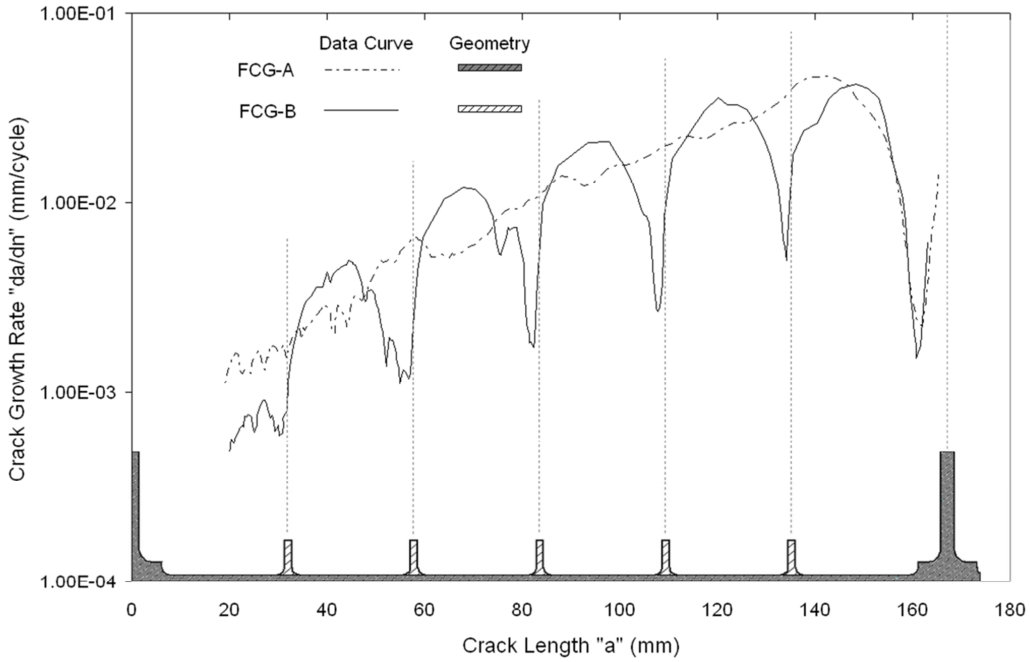


**Figure 7** Measured Crack growth rate for FCG-A and FCG-B.

A) FCG-A B) FCG-B C) FCG-E

**Figure 8** Captured images of the specimens at failure.

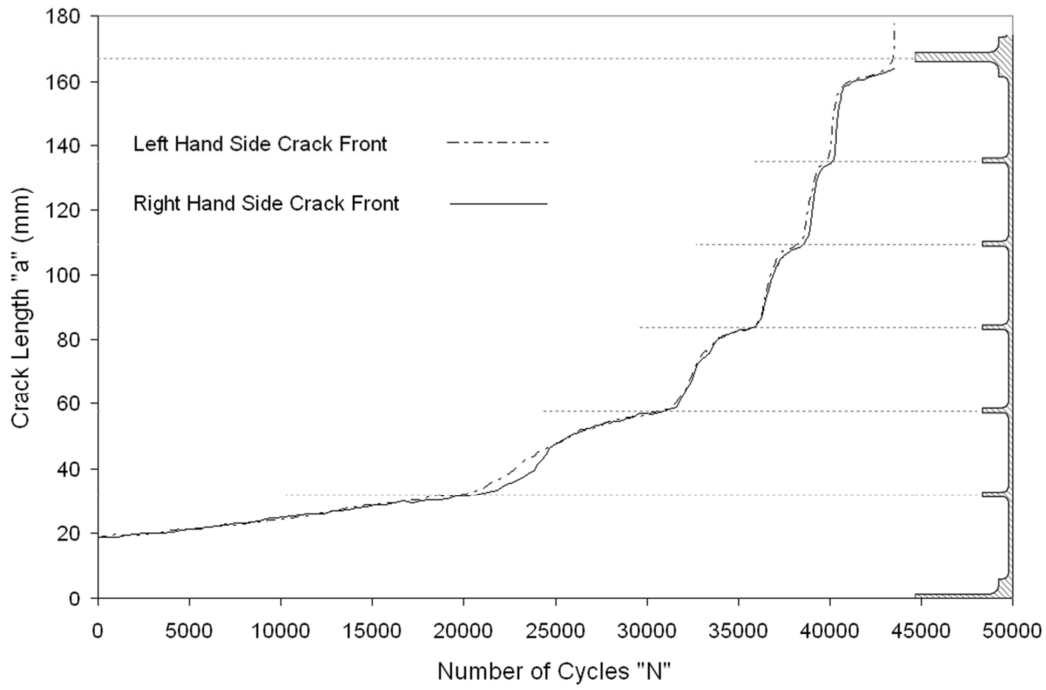


**Figure 9** Measured Crack propagation of the two crack fronts on FCG-B. Direction referenced from the stiffener side.

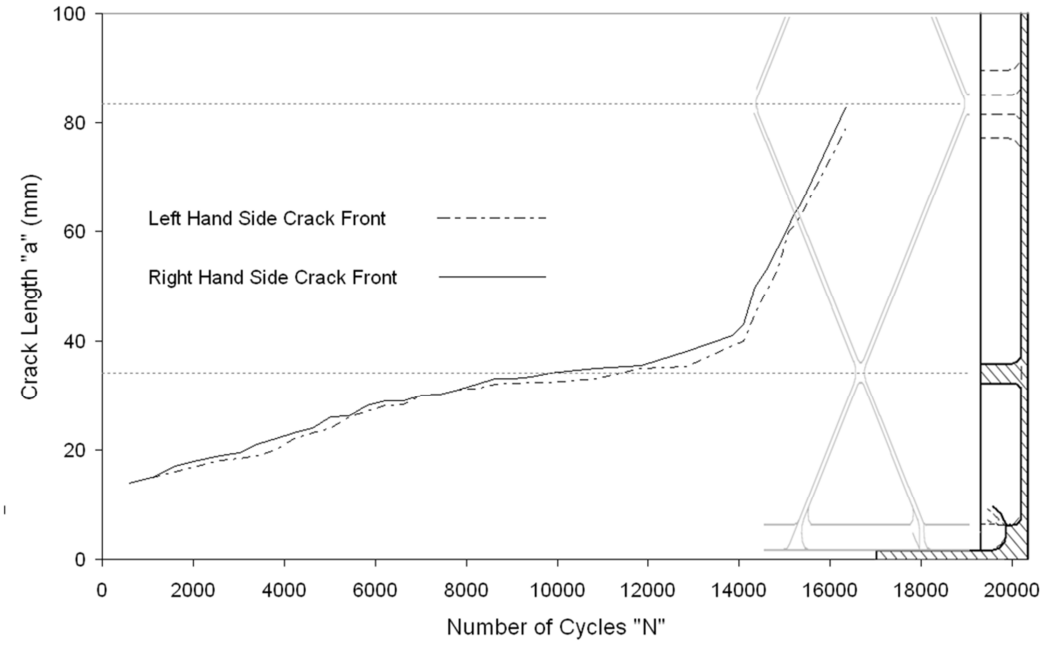


A) Primary Centre Crack

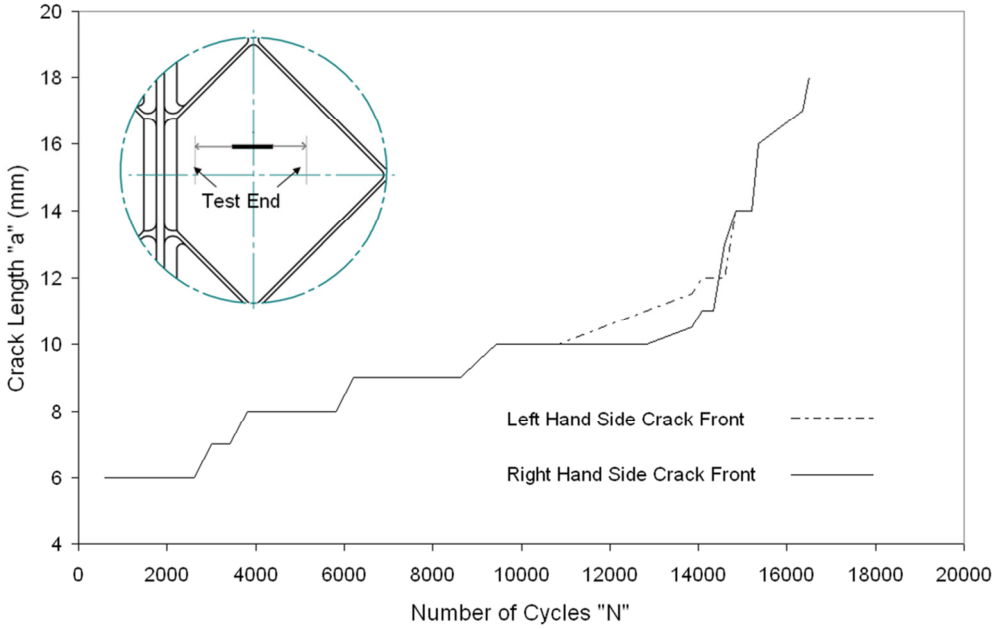


B) Secondary Edge Crack

**Figure 10** FCG-E crack lengths for both the left and right hand side crack fronts as measured from the central primary pre-damaged site and the secondary edge pre-damaged site. Crack directionality referenced from the specimen stiffener side.

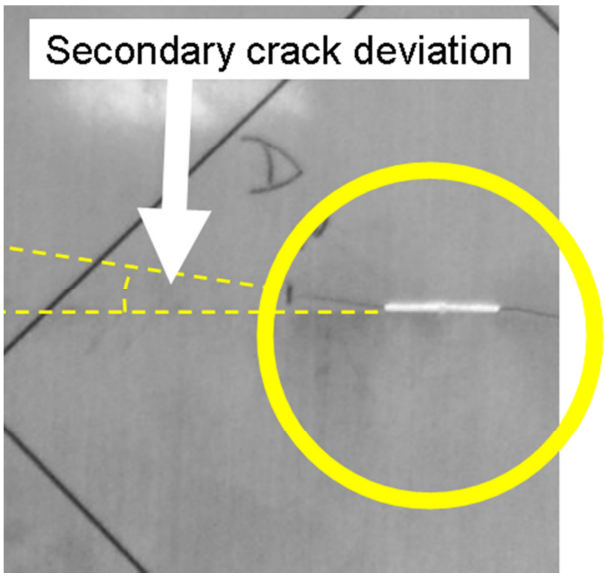


**Figure 11** FCG-E secondary crack directional deviation.

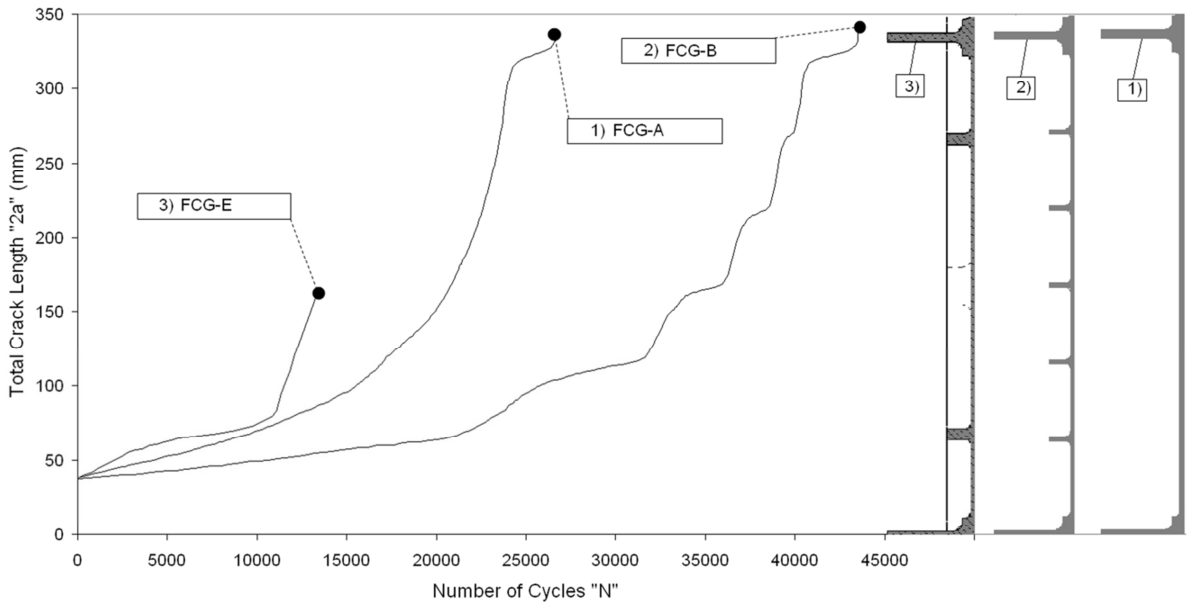


**Figure 12** Total crack lengths for all specimen primary pre-damaged sites, symmetrical about the central primary stiffener. Presentation of Specimen A and Specimen D data is corrected to facilitate an equivalent initial crack length with Specimen B.